

Damping of second sound in superfluid helium near T_λ

Michael J. Crooks and Bradley J. Robinson*

Department of Physics, University of British Columbia, Vancouver, British Columbia, V6T 2A6 Canada

(Received 29 July 1982)

The damping coefficient of second sound has been measured in liquid helium at saturated vapor pressure near T_λ . The results cover the temperature range $40 \text{ mK} > T_\lambda - T > 40 \text{ } \mu\text{K}$, and were obtained by the measurement of decay rates in a high- Q second-sound resonant cavity. These values are in good agreement with the predictions of nonlinear renormalization-group analysis applied to the asymmetric planar spin model for liquid helium in the "crossover" and precritical temperature ranges.

INTRODUCTION

In recent years measurements near the superfluid transition in liquid helium ($T_\lambda = 2.172 \text{ K}$) have provided a variety of critical tests and powerful stimuli for the developing theory of continuous phase transitions in solids and liquids. There have been several reviews of this particularly successful interaction of theory and experiment,¹⁻⁶ and the uniqueness of liquid helium as a testing ground has been described by Ahlers³ as follows:

"For the purpose of obtaining quantitative measurements extremely near a phase transition there is no other known system as suitable as ^4He . The sample is virtually free of the inhomogeneities which occur in many other systems in the form of impurities and strains for instance. The effect upon the transition of the gravitational field in which we do our experiments is relatively weak and well understood. The material has reasonably short thermal relaxation times which makes it possible to obtain measurements at equilibrium on a reasonable time scale. The transition occurs at a temperature at which the techniques of high resolution thermometry are very advanced. The transition temperature can be determined with very high resolution by noting the onset of thermal resistance in the fluid. We are able to study the transition as a function of pressure and ^3He concentrations. Thus, we have an entire plane of phase transitions at our disposal. And finally, the nature of the transition is such that by symmetry the experiments are always done on the coexistence curve. Whereas some of these advantages prevail also for other systems, no other phase transition can lay claim to all of them."

The need for further measurements of the attenuation of second sound near T_λ and the calculation from them of the damping coefficient has be-

come clear in recent years. The pioneering measurement of Hanson and Pellam⁷ do not extend sufficiently close to T_λ . Later measurements⁸ are in agreement with the predicted temperature dependence close to the transition, but disagree in magnitude with theoretical expectations. However, improved experiments by Ahlers⁹ over a restricted temperature range give results completely consistent with the predictions. Recent theoretical developments^{5,6,10-12} make it clear that the true asymptotic critical temperature range for dynamic phenomena near T_λ is much smaller than had been thought and is still experimentally unattainable. However, these same developments lead to quantitative predictions for the second-sound damping coefficient in the temperature range which is accessible and over a larger range than was previously possible.

The measurements reported here, which extend from $\Delta T = T_\lambda - T \simeq 40 \text{ } \mu\text{K}$ out to $\sim 40 \text{ mK}$ where they overlap the results of Hanson and Pellam, were briefly reported in Ref. 13. They appear to vindicate the application of nonlinear renormalization-group techniques using a nonisotropic spin model to an analysis of the dynamics of liquid helium near the superfluid transition.^{10(c)}

THEORY

A plane second-sound wave traveling in the z direction in superfluid helium is attenuated according to $\exp(-\alpha_2 z)$, where α_2 is the attenuation coefficient of the liquid. The damping coefficient D_2 for a wave of angular frequency ω is defined by

$$\alpha_2(\omega, T) = \frac{1}{2}(\omega^2/u_2^3)D_2(T), \quad (1)$$

where u_2 is the second-sound velocity. For linearized hydrodynamics, D_2 is independent of frequency and depends on such properties as the fluid viscosities, thermal conductivity, and the superfluid densi-

ty.¹⁴ For a plane standing wave, the power, after the excitation ceases, decays as $\exp(-t/\tau)$, where the time constant τ is related to the total attenuation α by

$$\frac{1}{\tau} = 2u_2\alpha. \quad (2)$$

Until recently, it was thought that measurements of dynamic properties of ^4He , taken in the reduced temperature range $\epsilon = (T_\lambda - T)/T_\lambda \leq 3 \times 10^{-4}$, would provide tests of asymptotic theories of critical dynamics. However, it is now realized that true asymptotic behavior occurs only at values of ϵ much smaller than those which can be reached, and calculation of the dynamic properties in the observable temperature range requires the inclusion of cross-over terms which provide corrections to the asymptotic scaling theory and extend the region of validity to the "precritical" range. This approach was first developed by Ferrell and Bhattacharjee.¹⁵ A quantitative treatment has been developed using the techniques of nonlinear renormalization-group theory in the two-loop approximation,^{5,6,10-12} and these techniques have been applied to the asymmetric planar spin model (model *F*) appropriate to liquid helium.² The current state of the theory has recently been reviewed.^{6,16}

Based on ^4He hydrodynamics, one writes the coupled Langevin equations for the entropy density $m(x, t)$ and the complex order parameter $\psi(x, t)$,

$$\begin{aligned} \dot{m} &= \lambda_0 \nabla^2 \frac{\partial H}{\partial m} + 2g_0 \text{Im} \left[\psi^* \frac{\partial H}{\partial \psi^*} \right] + \theta_m, \\ \dot{\psi} &= -2\Gamma_0 \frac{\partial H}{\partial \psi^*} - ig_0 \psi \frac{\partial H}{\partial m} + \theta_\psi, \end{aligned} \quad (3)$$

where

$$\begin{aligned} H &= \int d^3x \left(\frac{1}{2} r_0 |\psi|^2 + \frac{1}{2} |\nabla \psi|^2 + u_0 |\psi|^4 \right. \\ &\quad \left. + \frac{1}{2} m^2/c_{p0} + \gamma_0 m |\psi|^2 \right). \end{aligned} \quad (4)$$

Here λ_0 (real) and Γ_0 (complex) are the kinetic coefficients, g_0 , r_0 , u_0 , c_{p0} , and γ_0 are real constants, and θ_m and θ_ψ are Gaussian noise sources. The behavior of these equations can be conveniently described in terms of a parameter representing the ratio of the relaxation rates $w_0 \equiv \Gamma_0 c_{p0} / \lambda_0$ and a dimensionless coupling constant $f_0 \equiv g_0^2 \xi_0 / 2\pi^2 \Gamma_0 \lambda_0$, where ξ_0 is the amplitude of the correlation length. In the asymptotic region these parameters take on values w^* and f^* , and the universal amplitude ratio

$$R_2 \equiv \frac{1}{2} D_2 / u_2 \xi_t \quad (5)$$

is given by

$$R_2 = A (w^* f^*)^{-1/2} [1 + w^* + O(f^*)]. \quad (6)$$

Here ξ_t is the transverse correlation length and A is a constant depending on the static properties.

In the nonasymptotic regime, one may calculate a nonuniversal effective amplitude

$$R_2^{\text{eff}} = A [w(\epsilon) f(\epsilon)]^{-1/2} [1 + w(\epsilon)], \quad (7)$$

and this quantity is related to the second-sound damping over the same temperature range by

$$D_2 = 2R_2^{\text{eff}} u_2 \xi_t. \quad (8)$$

The approximate agreement of the temperature dependence of earlier data^{8,9} for $\epsilon \lesssim 10^{-3}$ with the predictions of asymptotic scaling is explained by the weak variation of R_2^{eff} with temperature in this range.

EXPERIMENT

The technique used in the present experiment was chosen in order to fulfill a number of requirements and will be described in more detail elsewhere.¹⁷ To approach T_λ as closely as possible and achieve a resolution in ΔT of the order of a few microkelvin, a resonant technique seemed desirable. It was necessary to use a short sample to reduce the effect of gravity¹⁸ on T_λ within the resonant cavity and simplify the problem of thermal isolation. A resonance method also provides a continuous-wave narrow-band signal to which powerful detection methods can be applied, and the resonance itself results in considerable amplification of the excitation signal. It was therefore possible to use a very small excitation level and reduce both the dc heat flow associated with it and the finite amplitude effects which can become serious close to T_λ , due to the vanishing of the superfluid density.

In essence, the procedure was to excite a plane-wave second-sound resonance in a small cylindrical cavity and record its decay after the excitation was switched off. The time constant for the decay was determined and led to values of attenuation which were much less sensitive to the ultimate temperature stability of the sample than those deriving from techniques which rely on measurement of the frequency width of resonance peaks. This procedure, though a well-established technique for measuring absorption effects, had not been applied previously to second sound in liquid helium. It proved crucial in obtaining the present results.

The resonant cavity consisted of two quartz optical flats parallel to within a few wavelengths of light, separated by a thin stainless-steel annulus (inside diameter 14.8 mm, length 3.0 mm). Second sound was generated thermally using a thin resistive

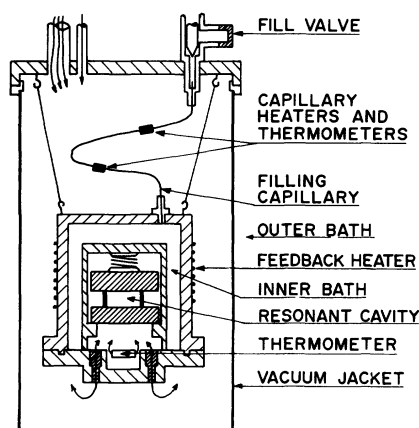


FIG. 1. Experimental cell. The outer bath was held below T_λ and was stable to better than 1 mK. The inner bath was stabilized to $\pm 2 \mu\text{K}$ and could be pumped slowly through a capillary line which is not shown.

metallic film evaporated onto the lower end piece and detected by an evaporated gold-lead film having a normal to superconducting transition spanning the temperature region of interest. This design helped minimize energy losses due to reflections at the surfaces of the cavity and produced a cell with $500 < Q < 1500$.

A simplified version of the experimental cell is shown in Fig. 1. The outer bath was stabilized at a temperature just below T_λ . The sample cell stability of $\pm 2 \mu\text{K}$ was obtained with a conventional feedback system. Resonances were excited at frequencies up to the fourth harmonic of the cell ranging from 100 Hz–5 kHz. Heat dissipation in the generator and detector led to the interior of the resonant cell being at a slightly higher temperature than the stabilized inner bath. Because of this effect, and because the calibration of the thermometer drifted slightly with time, the value of ΔT for each measurement was determined from the velocity of second sound within the resonator.

The typical maximum amplitude for the second-sound resonance was 10^{-7} – 10^{-8} K. The decaying amplitude was recorded using a high-sensitivity lock-in amplifier and averaged for a large number of decays to reduce the effects of thermal and electrical noise. An averaged decay curve is shown on both linear and semilogarithmic scales in Fig. 2. From the slopes of the semilogarithmic plots the decay rates $1/\tau$ for the signals were determined.

At a fixed value of ΔT decay curves were obtained for up to four harmonics. Decays were also obtained at several generator powers at each value of ΔT to allow extrapolation of the rates to zero power and therefore zero amplitude when providing values for analysis.

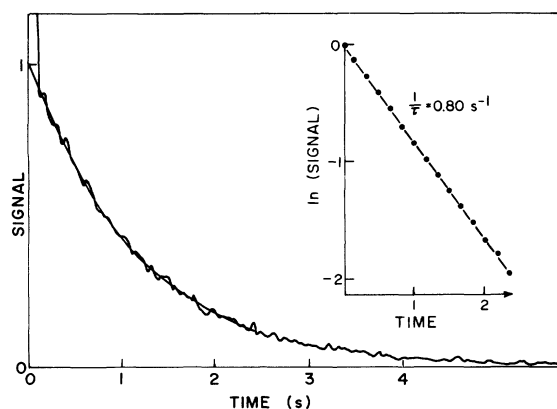


FIG. 2. Typical resonance decay. The initial very sharp decrease in signal strength was caused by a switching transient. The curve is the average of 150 decays.

Two effects on $1/\tau$ could be noticed when the dc detector power was varied. The first was a slight curvature of the semilogarithmic decay curve at sufficiently high detector powers. The system was always operated so that this effect was negligible. In addition, at each value of ΔT there was a detector power where a much enhanced decay of the resonance occurred. This “singular” power decreased at smaller ΔT values and “normal” decay rates could always be obtained by making measurements at powers well removed from these singular values. The source of this anomalous energy loss has not been identified.

ANALYSIS OF RESULTS

The main goals in the analysis of the measured decay times were to ensure that the resulting values of attenuation were representative of the bulk liquid and were capable of being described by linear superfluid hydrodynamics. All results were measured at low amplitudes where no signal-power dependence was detected or, if such dependence was unavoidable, results were extrapolated to zero signal power. A typical extrapolation is shown in Fig. 3 where the results for various detector powers are also indicated.

In addition to the absorption of energy from the resonant signal by the bulk helium in the cavity, there were energy losses at the chamber boundaries due to the viscous drag on the normal component near the cylindrical walls and to the finite thermal conductivities of both the stainless-steel side wall and the quartz end pieces. All these contributions were estimated, though the values ultimately used in the data analysis were determined using their dependence on frequency rather than by subtracting the calculated corrections.

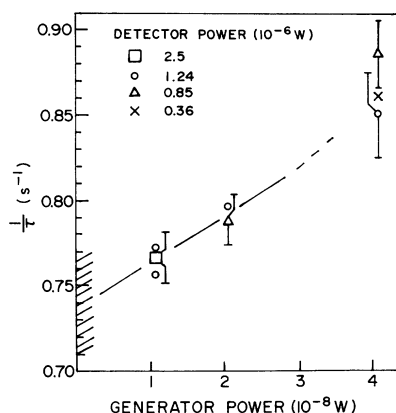


FIG. 3. Typical extrapolation of values for $1/\tau$ to zero generator power for different levels to detector power. The extrapolation to zero excitation power is used to estimate a best value for $1/\tau$. The hatched region indicates the error estimate.

Heiserman and Rudnick¹⁹ and Khalatnikov²⁰ have shown that for a second-sound wave in a cylindrical tube of radius r the viscous drag of the normal fluid at the wall leads to an attenuation

$$\alpha_\eta = (1/ru_2)(\rho_s/\rho)(\eta\omega/2\rho_n)^{1/2}, \quad (9)$$

where η is the normal fluid viscosity and ρ_s , ρ_n , and ρ are the superfluid, normal fluid, and total densities, respectively. The behavior of all relevant properties close to T_λ is known.¹

Khalatnikov²⁰ has also calculated the effective attenuation due to thermal conductivity of the side wall α_s and the end phase α_q . These are given by

$$\alpha_s = (2/rpcu_2)(c_s\kappa_s\omega/2)^{1/2} \quad (10)$$

and

$$\alpha_q = (2/apcu_2)(c_q\kappa_q\omega/2)^{1/2}, \quad (11)$$

where a is the length of the resonator, c is the specific heat of the helium, and c_s , c_q , κ_s , and κ_q are the heat capacities per unit volume and thermal conductivities of steel and quartz, respectively. This treatment assumes the effect of any Kapitza resistance at the bounding surface to be negligible. That assumption seems to be valid in the present case and is strengthened by the experimental results of Brow and Osborne,²¹ which indicate ac Kapitza resistances to be lower than those measured using dc thermal currents. In any case, the corrections were justified experimentally. Values calculated using Eqs. (10) and (11) at $\Delta T = 32$ mK give $1/\tau_\kappa$ within a factor of 2 of that determined experimentally, which may be considered quite satisfactory given the ap-

proximations necessary in determining the material properties.

The measured total decay rate $1/\tau$ may be considered to have contributions from bulk helium $1/\tau_{\text{He}}$, viscosity $1/\tau_\eta$, and conductivity effects at both walls and end plates $1/\tau_\kappa$. Thus one can write

$$\frac{1}{\tau} = \frac{1}{\tau_{\text{He}}} + \frac{1}{\tau_\eta} + \frac{1}{\tau_\kappa}. \quad (12)$$

In terms of the damping coefficient D_2 , the expression for $1/\tau_{\text{He}}$ is

$$\frac{1}{\tau_{\text{He}}} = 2u_2\alpha_2 = (\omega/u_2)^2 D_2 = (p\pi/a)^2 D_2 \quad (13)$$

for harmonic p . The essence of the method for obtaining $1/\tau_{\text{He}}$ is to use the difference in frequency dependence between the bulk contribution and the surface contributions. To enhance the graphical presentation of the data, it is useful to compute $1/\tau_\eta$ using Eq. (9). This contribution is significant for large ΔT . However, for $\Delta T < 1 \times 10^{-3}$ K it is small and comparable to or less than the error estimates on $1/\tau$. In addition, it is useful to decompose the bulk contribution as follows:

$$\frac{1}{\tau_{\text{He}}} = \frac{1}{\tau_{\text{HP}}} + \Delta \left[\frac{1}{\tau_{\text{He}}} \right]. \quad (14)$$

Here $1/\tau_{\text{HP}}$ denotes that value of $1/\tau_{\text{He}}$ which corresponds to the minimum value of D_2 ($3.58 \times 10^{-4} \text{ cm}^2 \text{ s}^{-1}$) from the results of Hanson and Pellam (at $\Delta T = 3.2 \times 10^{-2}$ K). Thus it is a constant which, using Eq. (13), is equal to $3.93 \times 10^{-2} \text{ s}^{-1}$ for harmonic one and $3.54 \times 10^{-1} \text{ s}^{-1}$ for harmonic three. $\Delta(1/\tau_{\text{He}})$ represents changes from this value. We now have $1/\tau - 1/\tau_\eta - 1/\tau_{\text{HP}}$, which is equal to $1/\tau_\kappa + \Delta(1/\tau_{\text{He}})$. Although it is necessary to correct the data of Hanson and Pellam to the T_{58} temperature scale,²² their values can be considered trustworthy in the sense that they use a method of measurement that yields α_2 directly. Their results indicate only small changes in D_2 over the temperature range $1 \times 10^{-2} < \Delta T < 5 \times 10^{-2}$ K. In that interval $\Delta(1/\tau_{\text{He}})$ is expected to be small and the reduced result can be used to check the validity of the predicted $\omega^{1/2}$ dependence for the surface losses. It should be emphasized that the subtraction of $1/\tau_\eta$ from $1/\tau$ is done only as a convenience in the graphical presentation to remove a large strongly temperature-dependent contribution at large ΔT . Also, the subtraction of $1/\tau_{\text{HP}}$ simply reduces the data by the appropriate constant value and provides a convenient way of displaying more clearly any changes, $\Delta(1/\tau_{\text{He}})$ from the minimum value obtained by Hanson and Pellam.

The resulting values of $1/\tau - 1/\tau_\eta - 1/\tau_{\text{HP}}$ are

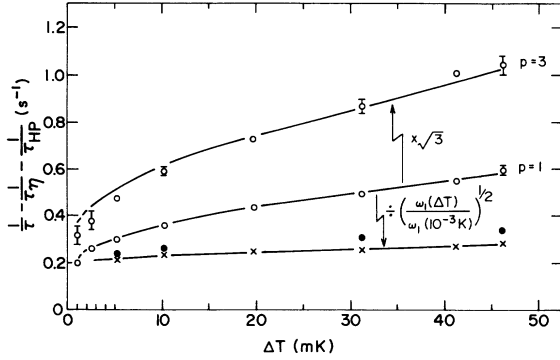


FIG. 4. Reduced decay rate $1/\tau - 1/\tau_\eta - 1/\tau_{HP}$ for $1 < \Delta T < 50$ mK. The viscous surface loss $1/\tau_\eta$ varies from 0.350 s^{-1} at 31 mK to 0.018 s^{-1} at 1 mK for harmonic one and is increased by a factor of $\sqrt{3}$ for harmonic three. The upper two solid lines are related by a factor of exactly $\sqrt{3}$. Also shown is the temperature dependence, relative to 1 mK, of the surface loss $1/\tau_\kappa$. The crosses represent the temperature dependence of the data and are derived from the values for the first harmonic by removing the frequency dependence. The solid circles represent the predicted values determined from the temperature dependence of the specific heat of helium.

shown in Fig. 4 for harmonics one and three for $1.0 \times 10^{-3} < \Delta T < 4.6 \times 10^{-2}$ K. The solid lines are meant as aids to the eye. The line drawn through the data points for $p=1$ yields, after multiplication by $\sqrt{3}$, the upper solid line for $p=3$. Since the major bulk attenuation contribution has been removed using the Hanson and Pellam data, it is expected that $\Delta(1/\tau_{He})$ is very small. Thus, on the basis of the good agreement between the $p=3$ data and the curve derived from the $p=1$ data, it is concluded that for the first and third harmonics, the contributions to $1/\tau$ from sources other than bulk damping are proportional to $\omega^{1/2}$.

The temperature dependence of the surface losses is indicated by the crosses in Fig. 4. This information is obtained as follows. The data for $p=1$ contains both a temperature and frequency dependence. The latter is removed by dividing by the factor $[\omega_1(\Delta T)/\omega_1(10^{-3} \text{ K})]^{-1/2}$, where $\omega_1(\Delta T)$ is the frequency of the first harmonic at ΔT . In this way the surface losses are normalized to the measured value at 1×10^{-3} K, and any variations reflect the temperature dependence. This treatment requires that the frequency dependence $\omega^{1/2}$ is correct and that any significant corrections from $\Delta(1/\tau_{He})$ in the data for $p=1$ are accounted for. The expected temperature dependence as predicted by Eqs. (10) and (11), due to the variation of the specific heat of helium, is indicated by the solid circles. Temperature

variations in the properties of the reflecting materials have been neglected, and would only account for a small fraction of the difference between the observed and predicted values. The source of the small discrepancy is not understood. It may be that the theory for $1/\tau_\eta$ or $1/\tau_\kappa$ is incomplete and that more consideration should be given to the details of the interface between the helium and the solid. In any case, by measuring $1/\tau$ for more than one harmonic at each temperature, knowledge of the temperature dependence is not required to obtain D_2 .

The values of $1/\tau - 1/\tau_\eta - 1/\tau_{HP} = 1/\tau_\kappa + \Delta(1/\tau_{He})$ for the first and third harmonics over the entire temperature range covered in this experiment are shown in Fig. 5. The enhanced damping at low ΔT is evidenced by the increase in the value of $\Delta(1/\tau_{He})$ for the third harmonic. For $\Delta T > 10^{-2}$ K, the error estimates are due to the fractional resolution (1% or 2%), in determining $1/\tau$ with large surface contributions present. At the three smallest values of ΔT it is clear that the error estimates are increasing rapidly as a result of the extrapolations resulting from the amplitude effects described above.

Since it is clear that all energy losses other than those due to bulk helium depend on $\omega^{1/2}$, it is possible to separate the two types of contributions unambiguously. The decay rates for the first and third harmonics are described by the expressions,

$$\begin{aligned} \left(\frac{1}{\tau} \right)_1 &= (D_2/u_2^2)\omega_1^2 + g\omega_1^{1/2}, \\ \left(\frac{1}{\tau} \right)_3 &= (D_2/u_2^2)\omega_3^2 + g\omega_3^{1/2}, \end{aligned} \quad (15)$$

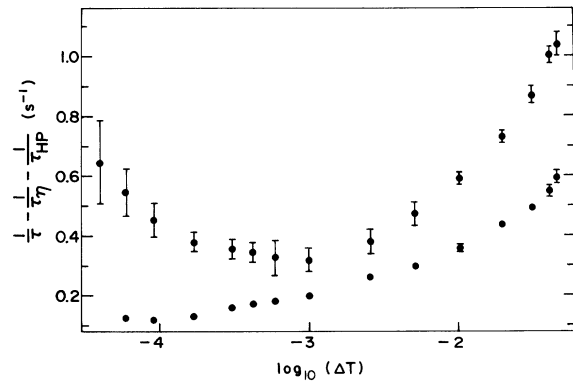


FIG. 5. Reduced decay rate $1/\tau - 1/\tau_\eta - 1/\tau_{HP}$ for harmonics one (lower points) and three (upper points) over the entire range of ΔT . The critical damping for $\Delta T < 10^{-3}$ results in the increasing separation of the data as $\Delta T \rightarrow 0$.

with $\omega_3 = 3\omega_1$. Here $g\omega^{1/2}$ represents all the surface contributions to the decay rate. Data for the first and third harmonics are used to solve Eqs. (15) for D_2 at each value of ΔT .

To determine ΔT within the resonator, the second-sound velocity was found from the measured fundamental frequency f_1 and resonator length. The velocity was then used to determine ΔT (when $\leq 2 \times 10^{-2}$ K) using²³

$$u_2 = f_1(2a) = 46.28 \left(\frac{\Delta T}{T_\lambda} \right)^{0.387}, \quad (16)$$

measured in m/s, and a graphical interpolation from the data of Greywall and Ahlers²⁴ was used for $\Delta T > 2 \times 10^{-2}$ K. Uncertainty in ΔT is the larger of $3 \mu\text{K}$ or 0.5% .

RESULTS AND CONCLUSIONS

Experimental values of D_2 plotted against ϵ are shown in Fig. 6. Also shown are the results of Ahlers⁹ and Hanson and Pellam.⁷ The latter are derived from the reported measurements of the attenuation using Eq. (1) and values of ϵ are determined after translating to the T_{58} temperature scale.²² The agreement among these data sets is especially satisfactory since in the experiments second sound was generated both thermally (present results and Hanson and Pellam) and using flexible porous filters (Ahlers). In each case D_2 was determined using a different technique: resonance decay (present results), resonant linewidth determinations (Ahlers), and amplitude versus distance measurements (Hanson and Pellam).

Experimental values of the amplitude ratio R_2 are shown in Fig. 7 where they are compared directly with theoretical values resulting from Eq. (7).^{10(c),25}

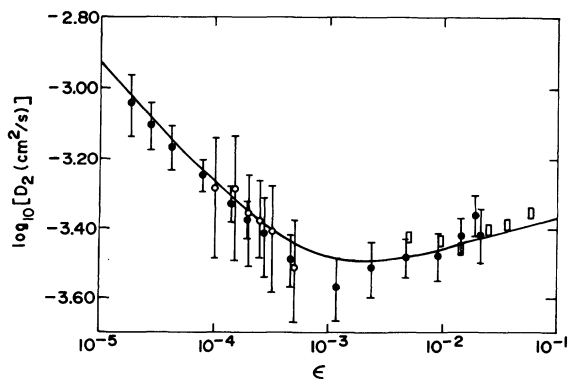


FIG. 6. $\log_{10} D_2$ vs ϵ ; ●, this work; ○, Ahlers; □, Hanson and Pellam. The solid curve shows the values of D_2 predicted (Ref. 6) using R_2^{eff} .

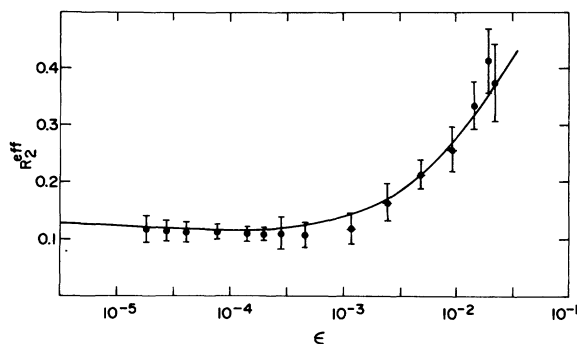


FIG. 7. Values of R_2^{eff} vs ϵ . The solid circles (●) show values calculated using values of D_2 as explained in the text. The solid curve shows model F calculated values (Ref. 6) with parameters fitted to the thermal conductivity data (Ref. 12) above T_λ .

The experimental points are derived from the D_2 data using Eq. (8), u_2 calculated from Eq. (16), and taking⁹

$$\xi_t = 3.57 \times 10^{-10} \epsilon^{-0.675}, \quad (17)$$

measured in m. The theoretical computations of R_2^{eff} are made^{10(c)} identifying certain nonuniversal parameters determining the behavior of w and f in Eq. (7) by using thermal conductivity measurements¹² made for $T > T_\lambda$. No further adjustable parameter is used.

These computed values of R_2^{eff} are used in conjunction with Eq. (8) and the values of u_2 and ξ_t to produce theoretical predictions for D_2 , shown by the solid line in Fig. 6. Agreement between theory and experiment is quite satisfactory.

The most recent theoretical work of Ferrell and Bhattacharjee²⁶ has also produced predictions for D_2 in the temperature range $\epsilon > 10^{-4}$ by using a "high-temperature" expansion. Their results differ significantly from the measured values, falling low for $\epsilon > 10^{-2.5}$. This approach would seem to require further refinement.

The existence of thermal conductivity data measured at $T > T_\lambda$ and pressures up to 29 bars makes it possible to extend quantitative theoretical predictions of D_2 .^{12,26} It is of considerable interest therefore to extend the measurements also.

ACKNOWLEDGMENTS

This research was supported by the Natural, Applied, and Health Sciences Grants Committee of the University of British Columbia. One of the authors (B.J.R.) would like to acknowledge financial support from the National Research Council of Canada and

from a Killam Fellowship. The authors are grateful to G. Ahlers, V. Dohm, and R. Folk for several useful conversations and particularly to W. Hardy for

first suggesting the technique of measuring decay rates.

*Present address: Department of Physics and Chemistry, University of Guam, Mangilao, Guam 96913.

¹G. Ahlers, in *The Physics of Liquid and Solid Helium Part I*, edited by K. H. Bennemann and J. B. Ketterson (Wiley, New York, 1976), Chap. 2.

²P. C. Hohenberg and B. I. Halperin, *Rev. Mod. Phys.* **49**, 435 (1977).

³G. Ahlers, in *Quantum Liquids*, edited by J. Ruvalds and T. Regge (North-Holland, Amsterdam, 1978).

⁴G. Ahlers, *Rev. Mod. Phys.* **52**, 489 (1980).

⁵P. C. Hohenberg, *Physica (Utrecht)* **109&110B**, 1436 (1982).

⁶V. Dohm and R. Folk, in *Festkörperprobleme, Advances in Solid State Physics*, edited by P. Grosse (Vieweg, Braunschweig, 1982), Vol. 22; *Physica (Utrecht)* **109&110B**, 1549 (1982).

⁷W. B. Hanson and J. R. Pellam, *Phys. Rev.* **95**, 321 (1954).

⁸J. A. Tyson, *Phys. Rev. Lett.* **21**, 1235 (1968).

⁹G. Ahlers, *Phys. Rev. Lett.* **43**, 1417 (1979).

¹⁰(a) V. Dohm and R. Folk, *Z. Phys. B* **35**, 277 (1979); (b) **40**, 79 (1980); (c) **45**, 129 (1981); (d) *Phys. Rev. Lett.* **46**, 349 (1981).

¹¹P. C. Hohenberg, B. I. Halperin, and D. R. Nelson, *Phys. Rev. B* **22**, 2373 (1980).

¹²G. Ahlers, P. C. Hohenberg, and A. Kornblit, *Phys. Rev. Lett.* **46**, 493 (1981); *Phys. Rev. B* **25**, 3136 (1982).

¹³M. J. Crooks and B. J. Robinson, 16th International Conference on Low-Temperature Physics, Los Angeles, 1981 [*Physica (Utrecht)* **107B**, 339 (1981)].

¹⁴See, for example, I. M. Khalatnikov, *An Introduction to the Theory of Superfluidity* (Benjamin, New York, 1965).

¹⁵R. A. Ferrell and J. K. Bhattacharjee, *Phys. Rev. Lett.* **42**, 1638 (1979); *Phys. Rev. B* **20**, 3690 (1979).

¹⁶See also the second part of Ref. 12.

¹⁷M. J. Crooks and B. J. Robinson, *Rev. Sci. Instrum.* **54**, 46 (1983).

¹⁸G. Ahlers, *Phys. Rev. A* **135**, 10 (1964); *Phys. Rev. Lett.* **10**, 439 (1963).

¹⁹J. Heiserman and I. Rudnick, *J. Low Temp. Phys.* **22**, 481 (1976).

²⁰I. M. Khalatnikov, *Usp. Fiz. Nauk* **60**, 69 (1956) (University of California Radiation Laboratory Translation 675).

²¹N. J. Brow and D. V. Osborne, *Philos. Mag.* **3**, 1463 (1958).

²²F. G. Brickwedde, H. van Dijk, M. Durieux, J. R. Clements, and J. K. Logan, *J. Res. Nat. Bur. Stand. Sect. A* **64**, 1 (1960).

²³See Ref. 1. From Eqs. 2.2.15 and 2.2.17.

²⁴D. S. Greywall and G. Ahlers, *Phys. Rev. A* **7**, 2145 (1973).

²⁵Similar plots comparing the present experimental results and also those of Refs. 7 and 9 to R_2^{eff} and D_2 derived from other model calculations are given in Fig. 22 of the second part of Ref. 12.

²⁶R. A. Ferrell and J. K. Bhattacharjee, *Physica (Utrecht)* **107B**, 341 (1981); *Phys. Rev. B* **24**, 5071 (1981).